Effect of Co and Ni doping on Structural, Optical and Vibrational Properties of CeO_2

Saurabh Tiwari[1, a)], Nasima Khatun[2, b)], Somaditya Sen[1, 2, c)]

[1]*Metallurgical Engineering and Material Sciences, Indian Institute of Technology Indore, India*
[2]*Department of Physics,Indian Institute of Technology Indore, India*

c)Corresponding author: sens@iiti.ac.in
b) phd1401151011@iiti.ac.in
a)phd1501181003@iiti.ac.in

Abstract. $Ce_{0.975}A_{0.025}O_2$ (A=Co, Ni) was synthesized using sol-gel method. X-ray diffraction (XRD), UV-Vis and Raman spectroscopy are employed to evaluate structural, optoelectronic and vibrational properties of samples. XRD and Raman analysis confirms substitution of Co and Ni in CeO_2 host matrix. It is observed that Co doping cause more strain and structural disorder than Ni doping in CeO_2. This is also reflected from crystallite size of samples. A broad Raman band emerges at ~ 540-650 cm^{-1} indicating increase in oxygen vacancies with doping. X-ray absorption near edge structure (XANES) analysis estimates oxygen vacancies and valance state of Ce (Ce^{3+}/Ce^{4+}) in CeO_2.

INTRODUCTION

In recent time cerium oxide-based nano-materials has attracted great attention. Transition metal doping is very effective tool for tuning various properties of nano-materials like structural, optical, electrical, and magnetic etc. Versatile applications like catalysis, biomedical, solid oxide fuel cells, gas sensors and oxygen storage[1–5] has been reported. Channei*et.al* reported enhanced photocatalytic activity with Fe doping in CeO_2[6], Ranjith, *et.al* reported ferromagnetism increases of CeO_2 with Co doping[7], Abbas *et.al* reported enhanced anticancer activity of CeO_2 with Ni doping[2]. But very less work has been reported on comparative analysis of transition elements in CeO_2.

In present work, we have studied 2.5% Co or Ni substituted CeO_2 nanoparticles synthesized by sol-gel technique. The structural, optical and vibrational properties have been investigated with the help of X-ray Diffraction (XRD), UV-Vis DRS (Diffused reflectance spectroscopy) and Raman spectroscopy. This work is a comparative study of lattice distortion and strain along with changes in Ce oxidation state (Ce^{3+}/Ce^{4+}) in Co and Ni added CeO_2.

EXPERIMENTAL

Cerium (III) nitrate hexahydrate [{$Ce(NO_3)_3.6H_2O$}; 99.9%, Alfa Aesar], Cobalt (II) nitrate hexahydrate [{$Co(NO_3)_2.6H_2O$};99.9%, Alfa Aesar], and Nickel (II) nitrate hexahydrate [{$Ni(NO_3)_2.6H_2O$};99.9%, Alfa Aesar] were dissolved in double distilled de-ionized water. The detailed synthesis procedure has been reported in our previous work[8].A black powder that was obtained was further calcined at 450°C for 6 h. CeO_2 and $Ce_{0.975}A_{0.025}O_2$ (A=Co or Ni) samples were prepared and coded as S1, S2 and S3 for (x=0, y=0; x=0.025, y=0 and x=0, y=0.025) respectively.

Bruker D2 Phaser X-ray Diffractometer was used for investigating structural properties of nanoparticles. Shimadzu UV-vis spectrophotometer (UV-2600) used for UV-vis diffused reflectance spectroscopy (DRS) analysis. Raman Micro Spectrometer, (HORIBA Scientific, excitation wavelength 632.8 nm) was used for Raman analysis. XANES measurements on the samples at Ce L_3-edge have been carried out at room temperature at EXAFS beamline (BL-9) at INDUS-2 synchrotron source (2.5 GeV, 300 mA) at RRCAT, Indore, India.

RESULT AND DISCUSSION

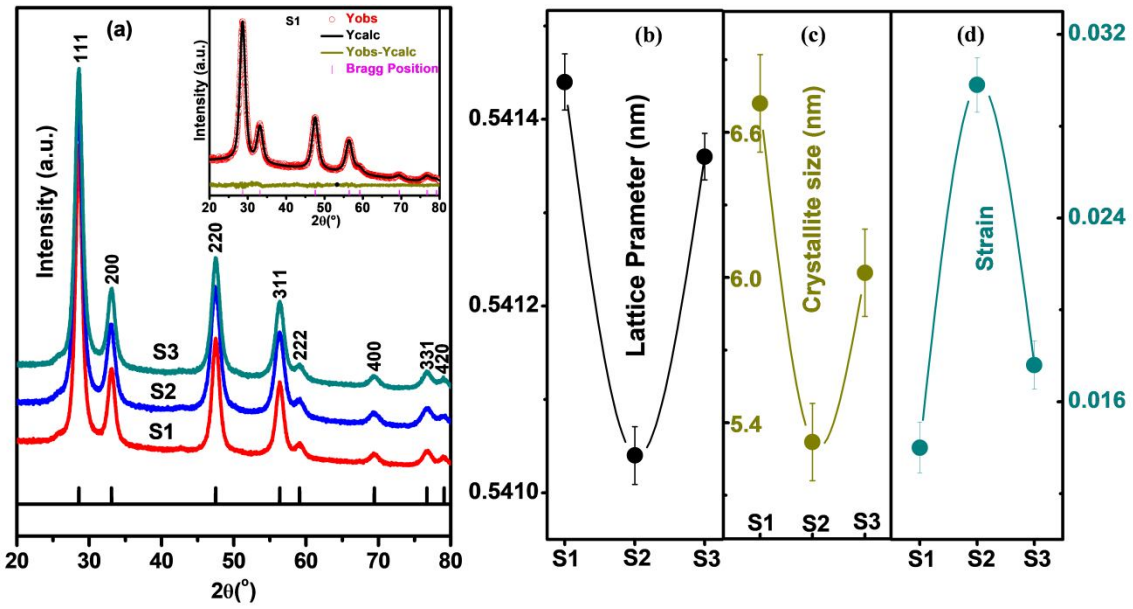

Fig.1. (a) XRD spectra of pure S1, S2 and S3 (inset shows Rietveld refinement of S1) (b, c, d) effect of Co and Ni doping on lattice parameter, crystallite size and strain of CeO_2.

XRD analysis reveals pure cubic fluorite phase formation of samples S1, S2 and S3 (Cif file-4343161; Crystallography open database). No oxide impurity phases of Co or Ni are present which confirms doping of Ce by Co and Ni [fig. 1 (a)]. Reitveld refinement [fig. 1 (a) inset] was performed using GSAS which reveals decrease in lattice parameter with substitution [fig. 1 (b)]. The crystal radius of Ce^{4+}(VIII) is ~1.11 Å which is being substituted by comparatively smaller $Co^{2+/3+}$(VIII) (~1.04-0.9Å) and $Ni^{2+/3+}$(VIII) (~0.95-0.83Å). Moreover, the lower ionic charge will result in some loss of oxygen from the lattice creating oxygen vacancies, V_O, thereby resulting in lattice strain and contraction of lattice. Hence, lattice parameters should reduce.

Increased amount of V_O may lead to transformation of a Ce^{4+} to a larger Ce^{3+}(VIII) (1.283 Å) ion[6]. Due to the larger size of Co as compared to Ni, V_O will be more in S2 than S3, resulting in more decrease in lattice parameter [Fig. 1 (b)] in CeO_2. The larger size of Co probably prevents a larger Ce^{3+} ion formation. Contraction in lattice leads to lattice distortion which causes lattice strain. Lattice strain was estimated from Williamson-Hall equation: $\beta*\cos\theta/\lambda = 1/D + \eta*\sin\theta/\lambda$ [9] where, D is the effective crystallite size, θ is diffraction angle, λ is wavelength of x-ray diffractometer, β is full width at half maxima (FWHM) of the XRD peaks and η is induce strain in lattice. Co doping shows higher strain than Ni [fig. 1 (d)] which also reflect in crystallite size [Fig.1 (c)].

Absorption spectra (UV-vis DRS) shows decrease in bandgap due to Co/Ni doping in CeO_2 samples [Figure 2 (a)]. Kubelka-Munk function used for estimating the bandgap[10], $F(R) = (1-R)^2/2R$. Bandgap of CeO_2 (S1) is 3.19 eV, which decreases to 2.85, 2.92 eV for S2 and S3 respectively [Figure 2 (b)]. Doping may create impurity bands (Ce^{3+} states and oxygen vacancies), between valance band (VB) and conduction band (CB)[11]

. Urbach energy was calculating to estimate lattice disorder (E_U): $\alpha = \alpha_0 * \exp(E/Eu)$, where, α is absorption coefficient. E_U is calculated by fitting a straight line to natural logarithm plot of the absorption edge (i.e. tailing part of absorption spectra). Defect states increase with substitution [Figure 2(b)] and higher in Co substitution. Decrease in bandgap is due to formation of new defect states which lowers the effective gap between VB and CB.

Raman phonon modes modify due to presence of dopants and disorder. CeO_2 has cubic fluorite structure with an F_{2g} symmetrical stretching mode, where oxygen atoms vibrate around Ce cations. S1 has F_{2g} mode at 462.48 cm^{-1} which red shifted with Co/Ni substitution [Fig. 3 (a, b)].The mode becomes broader with substitution [Fig. 3 (b-c)] indicating decrease of crystallite size and increase in strain. A broad peak at ~ 540-650 cm^{-1} attributed to oxygenvacancies intensify with substitution. Since $Co^{2+/3+}$ and $Ni^{2+/3+}$ have lower charge than CeO_2 (Ce^{4+}) hence to maintain charge neutrality oxygen vacancies in lattice increases.

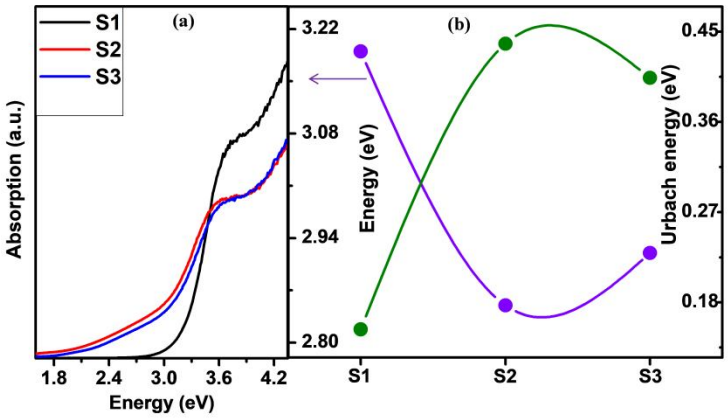

Fig. 2. (a) UV-Vis absorption spectra of S1, S2 and S3 (b) Variation of bandgap and Urbach energy with Co/Ni doping

Room temperature Ce L_3 XANES edge (transmission mode) reveals a mixed state of Ce. XANES spectra were similar for all samples and were fitted by a combination of an arctangent and four Gaussian peaks, A (~5730.9eV), B (~5724.1eV), C (~5719.3eV) and D (~5712 eV). A, B → mixture of multi-electron with final states of 2p4f05d* and 2p4f15d*L, where 2p refer to a Ce 2p hole, while 5d* refer to excited electron in 5d state and L refer to a hole in anion ligand orbital (O 2p), in Ce^{4+} valance state. C → Ce in Ce^{3+} valance state. D → final states of 2p5d due to crystal field splitting of Ce 5d states cause delocalization of d character at the bottom of the conduction band[11]. Quantification of Ce valence states was determined using area ratio of Ce^{3+} (C) and Ce^{4+} (A+B) as[12]: $[Ce^{3+}] = [C / (A+B+C)]*100$ and $[Ce^{4+}] = [(A+B) / (A+B+C)]*100$

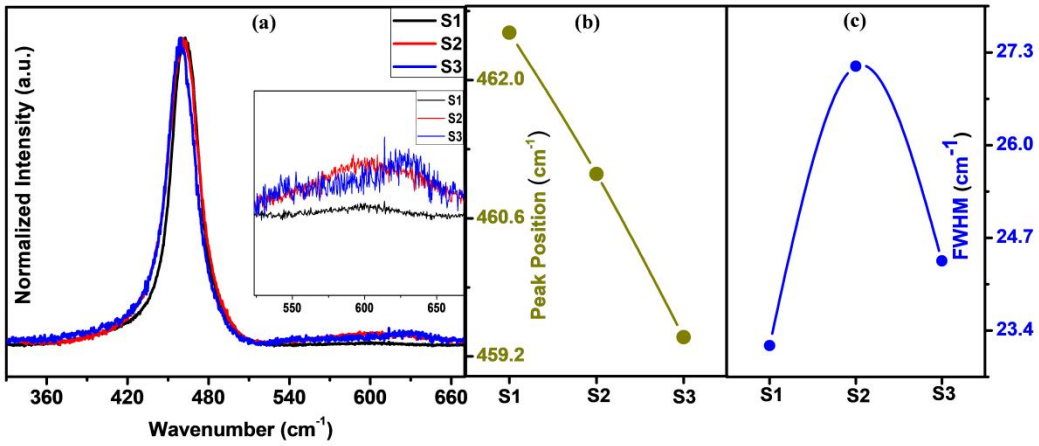

Fig 3. (a) Raman spectra of undoped (S1) and Co/Ni doped CeO_2 (S2&S3); (b-c) Change in peak position and in FWHM.

Analysis of the XANES data confirms presence of Ce in Ce^{4+} and Ce^{3+} states and increase of Ce^{3+} state with Co/Ni doping from 16.7% (S1) to 18.8% for Co substitution (S2) and 19.2% for Ni substitution (S3) respectively. This supports above analysis regarding higher strain in Co doped samples since in Ni doped Ce^{3+} concentration is higher which counteract the lattice contraction due to its larger size than Ce^{4+} which cause less strain.

CONCLUSION

$Ce_{0.975}A_{0.025}O_2$ (A=Co, Ni), samples were synthesized by sol-gel method. XRD shows pure phase formation and incorporation of Co/Ni in CeO_2. Co doping causes increase in strain and decrease in crystallite size than Ni. Reduction in bandgap is higher for Co (S2) substitution than Ni (S3); Urbach energy also confirms this since defects are higher with Co doping. Raman feature at ~540-650 cm^{-1} shows increase in oxygen vacancies related defects. XANES analysis shows Ce^{3+} concentration is higher for Ni substitution (S3) than Co (S2) which cause less disorder and strain in Ni doped CeO_2.

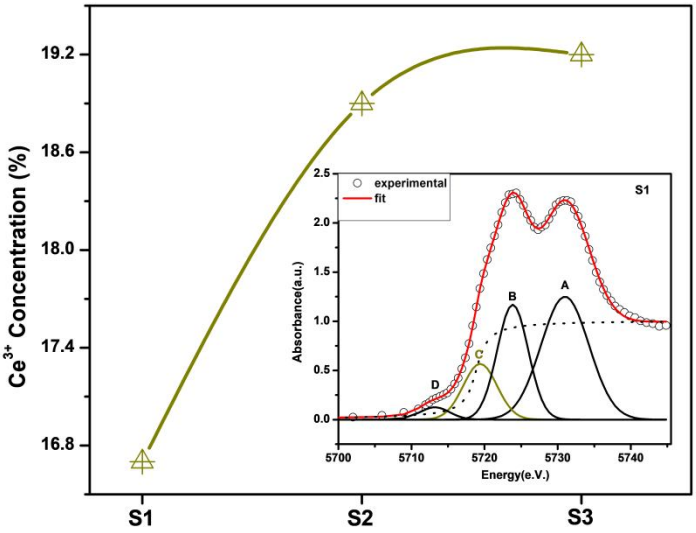

Fig. 4. Effect of Co/Ni substitution on Ce^{3+} concentration in CeO_2 (inset shows XANES spectra and fitting).

ACKNOWLEDGEMENTS

The authors would like to thank IIT Indore for the funding, Prof. A.L.Verma and Dr. V. K. Jain (Amity University, Noida, India) for UV-Vis measurement facility, Dr. S. Saha (IISER, Bhopal, India) for Raman spectroscopy of the samples and to Dr. S. N. Jha (RRCAT Indore) for providing XANES facility at BL-9. The first author thanks Dr. Swasti Saxena, for editing the draft.

REFERENCE

1. B. Murugan and A.V. Ramaswamy, J. Am. Chem. Soc. **129**, 3062 (2007).
2. F. Abbas, T. Jan, J. Iqbal, I. Ahmad, M.S.H. Naqvi, and M. Malik, Applied Surface Science **357**, 931 (2015).
3. K.C. Anjaneya, G.P. Nayaka, J. Manjanna, G. Govindaraj, and K.N. Ganesha, J. Alloys and Comp. **578**, 53 (2013).
4. P. Jasinski, T. Suzuki, and H.U. Anderson, Sensors and Actuators B: Chemical **95**, 73 (2003).
5. H. Imagawa, A. Suda, K. Yamamura, and S. Sun, J. Phys. Chem. C **115**, 1740 (2011).
6. D. Channei, B. Inceesungvorn, N. Wetchakun, S. Ukritnukun, A. Nattestad, J. Chen, and S. Phanichphant, Scientific Reports **4**, 5757 (2014).
7. K.S. Ranjith, P. Saravanan, S.-H. Chen, C.-L. Dong, C.L. Chen, S.-Y. Chen, K. Asokan, and R.T. Rajendra Kumar, J. Phys. Chem. C **118**, 27039 (2014).
8. S. Tiwari, G. Bajpai, T. Srivastava, S. Viswakarma, P. Shirage, S. Sen, and S. Biring, ScriptaMaterialia **129**, 84 (2017).
9. S. Tiwari, N. Khatun, P. Rajput, D. Bhattacharya, S.N. Jha, C.-M. Tseng, S.-W. Liu, S. Biring, and S. Sen, Appl. Phys. A **124**, 609 (2018).
10. S. Tiwari, N. Khatun, T. Shrivastava, S. Kumar, S.-W. Liu, S. Biring, and S. Sen, Superlattices and Microstructures **122**, 316 (2018).
11. J. Hays, A. Punnoose, R. Baldner, M.H. Engelhard, J. Peloquin, and K.M. Reddy, Phys. Rev. B **72**, 075203 (2005).
12. S. Phokha, S. Pinitsoontorn, and S. Maensiri, Nano-Micro Lett. **5**, 223 (2013).